Nanoplasmonics of prime number arrays

Carlo Forestiere,[1,3] Gary F. Walsh,[1] Giovanni Miano,[3] and Luca Dal Negro[1,2,*]

[1]*Department of Electrical and Computer Engineering & Photonic Center, 8 Saint Mary's Street, Boston, MA, 02215*
[2]*Division of Materials Science and Engineering, Boston University, Boston, MA, 02215, USA*
[3]*Department of Electrical Engineering, Università degli Studi di Napoli Federico II, Napoli, 80125, Italy*
**dalnegro@bu.edu*

Abstract: In this paper, we investigate the plasmonic near-field localization and the far-field scattering properties of non-periodic arrays of Ag nanoparticles generated by prime number sequences in two spatial dimensions. In particular, we demonstrate that the engineering of plasmonic arrays with large spectral flatness and particle density is necessary to achieve a high density of electromagnetic hot spots over a broader frequency range and a larger area compared to strongly coupled periodic and quasi-periodic structures. Finally, we study the far-field scattering properties of prime number arrays illuminated by plane waves and we discuss their angular scattering properties. The study of prime number arrays of metal nanoparticles provides a novel strategy to achieve broadband enhancement and localization of plasmonic fields for the engineering of nanoscale nano-antenna arrays and active plasmonic structures.

OCIS codes: (240.6680) Surface plasmons; (240.6695) Surface-enhanced Raman scattering; (050.6624) Subwavelength structures; (290.4020) Mie theory.

References and links

1. L. Dal Negro, N. N. Feng, and A. Gopinath, "Electromagnetic coupling and plasmon localization in deterministic aperiodic arrays," J. Opt. A, Pure Appl. Opt. **10**(6), 064013 (2008).
2. A. Gopinath, S. V. Boriskina, N. N. Feng, B. M. Reinhard, and L. Dal Negro, "Photonic-plasmonic scattering resonances in deterministic aperiodic structures," Nano Lett. **8**(8), 2423–2431 (2008).
3. R. Dallapiccola, A. Gopinath, F. Stellacci, and L. Dal Negro, "Quasi-periodic distribution of plasmon modes in two-dimensional Fibonacci arrays of metal nanoparticles," Opt. Express **16**(8), 5544 (2008).
4. A. Gopinath, S. V. Boriskina, B. M. Reinhard, and L. Dal Negro, "Deterministic Aperiodic Arrays of Metal nanoparticles for surface-enhanced Raman scattering (SERS)," Opt. Express **17**(5), 3741–3753 (2009).
5. S. G. Williams, *Symbolic dynamics and its applications*, (American Mathematical Society, 2004).
6. P. Prusinkiewicz, and A. Lindenmayer, *The algorithmic beauty of plants,* (Springer Verlag, 1990).
7. J. Mishra, and S. N. Mishra, *L-System Fractals,* (Elsevier, 2007).
8. M. R. Schroeder, *Number theory in science and communication*, (Springer Verlag, 1985).
9. G. H. Hardy, and E. M. Wright, *An introduction to the theory of numbers*, (Oxford University Press, 2008).
10. S. J. Miller, and R. Takloo-Bighash, *An Invitation to Modern Number Theory*, (Princeton University Press, 2006).
11. M. Queffelec, "Substitution dynamical systems-spectral analysis," (Springer, 1987).
12. E. Maciá, "The role of aperiodic order in science and technology," Rep. Prog. Phys. **69**(2), 397–441 (2006).
13. M. Dulea, M. Johansson, and R. Riklund, "Localization of electrons and electromagnetic waves in a deterministic aperiodic system," Phys. Rev. B Condens. Matter **45**(1), 105–114 (1992).
14. L. Dal Negro, and N. N. Feng, "Spectral gaps and mode localization in Fibonacci chains of metal nanoparticles," Opt. Express **15**(22), 14396 (2007).
15. C. Forestiere, G. Miano, G. Rubinacci, and L. Dal Negro, "Role of aperiodic order in the spectral, localization, and scaling properties of plasmon modes for the design of nanoparticle arrays," Phys. Rev. B Condens. Matter **79**(8), 85404 (2009).
16. L. Kroon, E. Lennholm, and R. Riklund, "Localization-delocalization in aperiodic systems," Phys. Rev. B Condens. Matter **66**(9), 094204 (2002).
17. A. Gopinath, N. Lawrence, S. Boriskina, L. Dal Negro, "Enhancement of the 1.54μm Erbium emission in aperiodic plasmonic arrays" in preparation.

#116360 - $15.00 USD Received 27 Aug 2009; revised 9 Nov 2009; accepted 9 Nov 2009; published 18 Dec 2009

18. C. Forestiere, G. Miano, S. V. Boriskina, and L. Dal Negro, "The role of nanoparticle shapes and deterministic aperiodicity for the design of nanoplasmonic arrays," Opt. Express **17**(12), 9648–9661 (2009).
19. C. Janot, *Quasicrystals: A Primer*, (Oxford University Press, 1997).
20. P. B. Johnson, and R. W. Christy, "Optical Constants of the Noble Metals," Phys. Rev. B Condens. Matter **6**(12), 4370–4379 (1972).
21. T. Matsui, A. Agrawal, A. Nahata, and Z. V. Vardeny, "Transmission resonances through aperiodic arrays of subwavelength apertures," Nature **446**(7135), 517–521 (2007).
22. M. R. Schroeder, "A simple function and its Fourier transform," Math. Intelligencer **4**(3), 158–161 (1982).
23. M. L. Stein, S. M. Ulam, and M. B. Wells, "A visual display of some properties of the distribution of primes," Am. Math. Mon. **71**(5), 516 (1964).
24. J. D. Johnston, "Transform Coding of Audio Signals Using Perceptual Noise Criteria," IEEE J. Sel. Areas Comm. **6**(2), 314 (1988).
25. L. Novotny, and B. Hecht, *Principles of Nano-Optics*, (Cambridge University Press, 2006).
26. C. Forestiere, A. Gopinath, G. Miano, L. Dal Negro, S. Boriskina, "Structural resonances in finite-size periodic plasmonic arrays," in preparation.
27. A. Alù, and N. Engheta, "Hertzian plasmonic nanodimer as an efficient optical nanoantennas," Phys. Rev. B Condens. Matter **78**(19), 195111 (2008).
28. L. Novotny, "Effective Wavelength Scaling for Optical Antennas," Phys. Rev. Lett. **98**(26), 266802 (2007).
29. M. I. Mishchenko, L. D. Travis, and A. A. Lacis, *Multiple scattering of light by particles: radiative transfer and coherent backscattering*, (Cambridge University Press, 2006).
30. J. D. Jackson, *Classical Electrodynamics*, (Wiley, 1998).

1. Introduction

Deterministic aperiodic (DA) arrays of metal nanoparticles have recently attracted a considerable interest due to their unique ability to strongly enhance and localize electromagnetic fields at multiple frequencies within engineered optical chips for nanoplasmonics applications [1–4]. DA structures are generated by the mathematical rules of symbolic dynamics [5], L-systems [6,7], and number theory [8,9], can be conveniently fabricated using conventional nano-lithographic techniques, and show great structural complexity resulting in multi-fractal energy spectra with localized eigenmodes [11–16]. Differently from conventional photonic-plasmonic crystals, which are constrained by translational invariance symmetry, DA arrays enable the flexible control of sub-wavelength gaps and localized field states. In particular, the great structural flexibility of DA arrays provides a unique opportunity for the engineering of novel light dispersion schemes, density of states fluctuations, radiation patterns, and localized field states with broad frequency spectra in non-periodic nanostructures amenable to predictive theories. Based on this approach, we recently demonstrated broadband plasmonic scattering [2], state of the art, reproducible Raman enhancement factors [4], and plasmon-enhanced light emission from silicon-based structures [17].

Until now, the study of the optical properties of DA structures with flat Fourier spectra has been limited to Rudin-Shapiro structures [1–4]. In this paper, we propose the first investigation in the context of nanoplasmonics of a fascinating category of aperiodic structures based on the distribution of prime numbers in two spatial dimensions (2D). These structures provide a general model to understand and to engineer nanoplasmonic arrays with structural properties approaching the complexity of spatial random processes with flat Fourier transform. Despite the exact distribution of prime numbers still remains unknown [8–10], large-scale prime number arrays can be deterministically generated and exhibit highly fluctuating, almost flat Fourier spectra which can be understood within the general framework of analytic number theory [9,10].

Specifically, in this paper, we will study three main types of prime number arrays: the coprime arrays, which are two-dimensional distributions of particles with coprime coordinates; the prime number arrays, which are two-dimensional arrays of particles representing prime numbers in reading order; and the Ulam spirals, which consist of prime numbers arranged on a square spiral. Our computational study is based on a recently developed coupled-dipole method [18], which is particularly suited to efficiently describe the optical properties of large-scale nanoparticles systems. We recently validated this method

#116360 - $15.00 USD Received 27 Aug 2009; revised 9 Nov 2009; accepted 9 Nov 2009; published 18 Dec 2009

against analytical theories [18] and found it appropriate to model a large number of dipolar nanoparticles with an accuracy comparable to the alternative methods of nanoplasmonics.

In this paper we will demonstrate that Fourier spectra with large spectral flatness are required to achieve plasmonic field enhancement effects over broader frequency ranges compared to strongly coupled periodic and Fibonacci quasi-periodic structures [3], which possess purely singular (point-like) Fourier spectra [19]. In addition, we will discuss the far-field scattering properties of prime number arrays illuminated by plane waves. Our findings make prime number arrays a particularly fascinating design concept for emerging technological applications such as plasmonic nano-antennas, broadband plasmonic solar cells and plasmonic-enhanced light-emitting nanostructures.

2. Prime Number Arrays

In this section, we will introduce the three main prime number plasmonic arrays and discuss their structural and spectral (Fourier) properties. Periodic (square lattice) and quasi-periodic Fibonacci plasmonic structures [3] are additionally investigated for comparison. All the investigated arrays consist of silver (Ag) spherical nanoparticles with radius r=50nm and d_{min}=25nm minimum edge-to-edge interparticle separation. The materials response of the nanoparticles has been modeled according to the dispersion data in Ref [20].

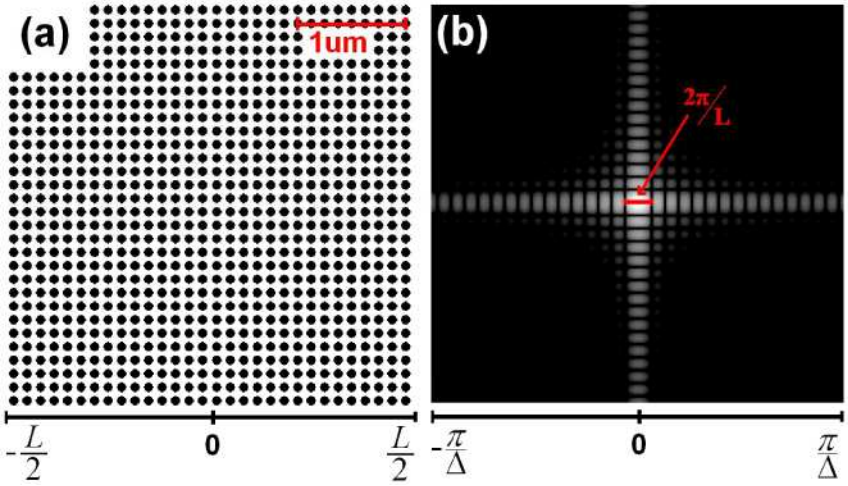

Fig. 1. Periodic array and its structure in the reciprocal space (logarithmic scale), where L = 3.75 and Δ is the center to center inter-particle distance, namely Δ = d_{min}+2r. The reciprocal space is obtained by the discrete Fourier transform (DFT). The width of the central peak in the reciprocal space is inversely proportional to the array's dimension.

In order to achieve a better understanding of the geometrical properties of the arrays, it is important to investigate the structure associated to their reciprocal vectors (reciprocal space), which can be obtained by the discrete Fourier transform (DFT) of the arrays [21]. By construction [1], the arrays are all defined by a two-valued function f_{nm} on a square grid. The function f_{nm} is equal to 1 if a particle occupies the position (n,m), 0 otherwise. We note that since the arrays are all bounded by a square aperture (finite-size arrays) of size L, the DFT of a square aperture (sinc function) will be convoluted with the geometry dependent Fourier structure (array patterns) of the arrays. As a result, the reciprocal space of a periodic finite-size array f_{nm} is equal to the discrete convolution between the DFT of the square aperture which limits the array size, and the DFT of the repeated function f_{nm} (array pattern) which positions the particles on a two dimensional square lattice. However, in this paper we will consider only the first Brillouin zone of the reciprocal square lattice, since it can be directly compared with the pseudo-Brillouin zones of the prime number arrays [14, 19]. These arrays

#116360 - $15.00 USD Received 27 Aug 2009; revised 9 Nov 2009; accepted 9 Nov 2009; published 18 Dec 2009

are not periodic, and a Brillouin zone cannot rigorously be defined. However, the so-called pseudo-Brillouin zones can be introduced by restricting the reciprocal vectors k_x and k_y in the range $-\pi/\Delta$ and π/Δ,,(Δ, is the minimum center-to-center distance between two consecutive particles, namely $\Delta=d_{min}+2r$).

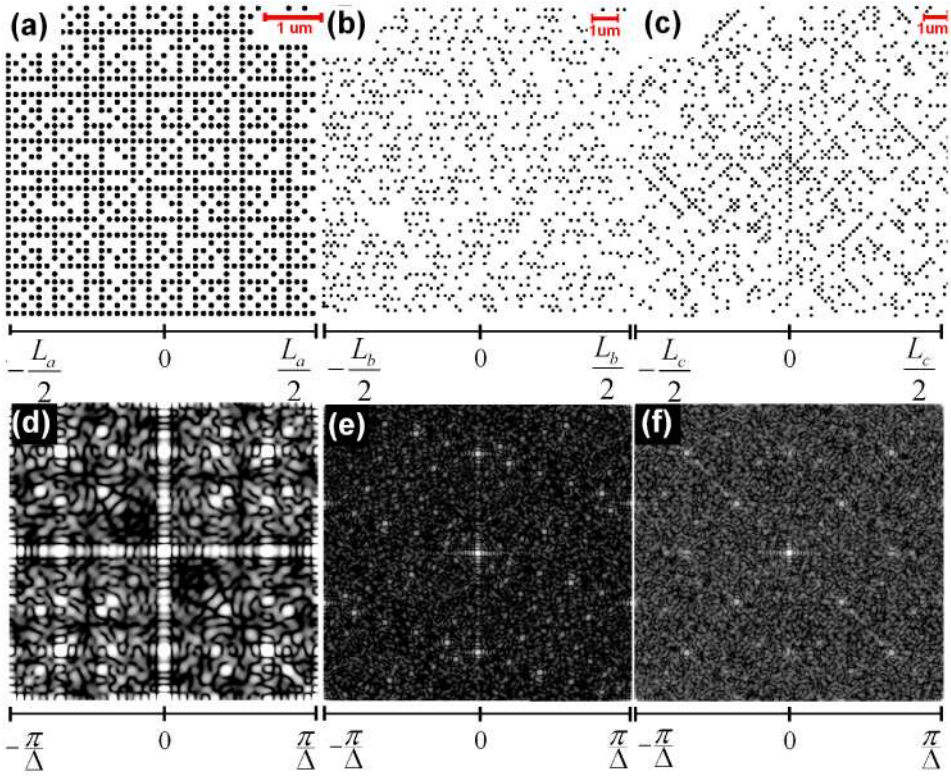

Fig. 2. Aperiodic arrays (a-c) and their corresponding structures in the reciprocal space (logarithmic scale) (d-f): (a) and (d) Coprime L_a=4.9μm, (b) and (e) Prime L_b=10.5μm, (c) and (f) Ulam L_c=11μm. The dimensions of the reciprocal space are the same as in the periodic case (Fig. 1(b)) since the minimum center to center inter-particle distance (Δ) is equal to the periodic case.

In Fig. 1(a) we show the periodic lattice and the first Brillouin zone associated to its reciprocal space (Fig. 1(b)). Coprime, prime number and Ulam spiral arrays are shown in Figs. 2 (a)-(c), while in Figs. 2 (d)-(f) we show their pseudo-Brillouin zones. The coprime array is shown in Fig. 2(a) and it is simply obtained by positioning metal nanoparticles in correspondence to each coprime pair of integers in the two-dimensional plane. Here we recall that two integers a and b are said to be coprime $(a \perp b)$ if their greatest common divisor GCD, denoted by (a,b), equals 1 (they have no common factors other than 1). Figure 2(d) shows the Fourier spectrum of the coprime array. We notice that since the array is symmetric around the 45° diagonal, so is the Fourier transform. Furthermore, since we plot the *magnitude* of the Fourier transform also the −45° diagonal will appear as a symmetry axis. In addition, we can notice in Fig. 2(a) that there are near symmetries about the horizontal and vertical axes, whose more complex nature is discussed in Ref. 22. Compared to the spectrum of the periodic structure shown in Fig. 1(b), the coprime features a broader spectrum of spatial frequencies. As reported in Table 1 the filling fraction of the coprime array is about ½ the periodic case, but the average nearest neighbor distance between nanoparticles, namely ($<d_{min}>$), is roughly the same. However, despite the first neighbor distance is almost equal to the periodic case, the number of nearest neighbors is much less. Further, the coprime lattice

#116360 - $15.00 USD Received 27 Aug 2009; revised 9 Nov 2009; accepted 9 Nov 2009; published 18 Dec 2009

features several characteristic length scales, one of each corresponding to the periodic distance d_{min}, the others ones are related to the most frequent distances between the first 40 prime numbers. As a consequence the coprime DFT shows several peaks in the first pseudo-Brillouin zone.

Table 1. – Geometric parameters describing the main characteristics of investigated arrays.

	Periodic	Coprime	Prime	Ulam
Spectral flatness (SF)	0.0009	0.6729	0.7858	0.8118
# Nanoparticles	961	979	960	1000
Linear dimension (L)	3.75μm	4.9μm	10.7μm	11.0μm
Particle density	$68.33\mu m^{-2}$	$41.51\mu m^{-2}$	$8.4\mu m^{-2}$	$8.3\mu m^{-2}$
Expected density	$68.33\mu m^{-2}$	$41.68\mu m^{-2}$	$8.82\mu m^{-2}$	$8.77\mu m^{-2}$
Filling fraction (FF)	0.536	0.324	0.065	0.065
$<d_{min}>$	25nm	27nm	117nm	111nm
d_{min}	25nm	25nm	25nm	25nm

In Fig. 2(b) we show the prime number array. This is built by arranging the first N^2 natural numbers on the rows of a $N \times N$ matrix in reading order (i.e. a serpentine) and by positioning Ag nanoparticles only in correspondence of prime number locations. The complexity of this pattern is described by an almost uniform Fourier spectrum with no detectable symmetries, as shown in Fig. 2(e). The last array that we considered is the Ulam spiral (Fig. 2(c)) which was discovered in 1963 by the polish mathematician Stanislaw Ulam while doodling on scrap paper at a scientific meeting. The Ulam spiral consists of a lattice of natural integers positioned on a square spiral where only prime numbers are plotted [23]. The positions of nanoparticles in the Ulam spiral appear correlated along the diagonal axis, which are also the only symmetry axis of the associated Fourier transform (Fig. 2(f)). It is currently unknown to number theorists why prime numbers appear to cluster along certain diagonals of the Ulam spiral [8,23].

Due to a larger size L of the prime and Ulam arrays, the ratio $2\pi/L$ is smaller compared to the coprime and the periodic case. This affects the fine features of the DFT of those arrays, since they are related to the distance between two consecutive zero–crossings of the sinc function associated to the limiting square aperture. Further since ($<d_{min}>$) is larger than in the periodic case the DFT of prime and Ulam lattices shows several peaks in the first pseudo-Brillouin zone.

The varying degree of structural complexity of the different arrays can be quantified by a parameter, called the spectral flatness (SF), associated to their Fourier spectra. The SF is a digital signal processing measure of how spectrally diffused a signal is. In our case, the different arrays are considered as digitized spatial signals and the SF is calculated by dividing the geometric mean and the arithmetic mean of their power spectra, according to the definition [24]:

$$SF = \frac{\sqrt[N]{\prod_{n=0}^{N-1}\left|\mathrm{DFT}\left\{s(n)\right\}\right|}}{\left(\frac{\sum_{n=0}^{N-1}\left|\mathrm{DFT}\left\{s(n)\right\}\right|}{N}\right)} \qquad (1)$$

where $s(n)$ is the value of the spatial signal (array) in bin n, N is the total number of bins in the array, DFT is the Discrete Fourier Transform, and $|\,|$ is the magnitude. For a signal with a completely flat power spectrum, the geometric mean will equal the arithmetic mean causing the SF to be equal to one. This indicates that there is equal power in every frequency band. If

#116360 - $15.00 USD Received 27 Aug 2009; revised 9 Nov 2009; accepted 9 Nov 2009; published 18 Dec 2009

there are frequencies with zero power, the geometric mean will be zero so SF will also be zero indicating a band limited signal.

In Table 1 we show the calculated SF values for all the arrays, which increase with the complexity of the Fourier spectra from periodic to prime number and Ulam structures. In addition to the SF values, the arrays also differ in their particle density (number of particles/area) and filling fraction (total particles areas/total array area). As will become clear later in the paper, these are two other important parameters which, in addition to the arrays spectral character, strongly affect the transport and localization properties of plasmonic fields.

It is very interesting to notice that, despite the complexity of prime number arrays, their density can be studied analytically in the limit of large structures. It is in fact a well know result of analytical number theory [9,10] that the probability of two randomly selected integers to be coprime is equal to:

$$\sum_{n=1}^{\infty}\frac{1}{n^2}=\varsigma(2)=\frac{6}{\pi^2}\approx 0.61 \tag{2}$$

where ς refers to the Riemann zeta function. This means that, once we choose the same minimum interparticle distance for a periodic and a coprime array, the density of coprime array will be 61% of the density of the periodic array.

Analytical number theory helps us in determining the asymptotic particle density of the prime number and Ulam spiral arrays as well. In fact, we recall that the number of primes smaller than or equal to an integer x defines a function called $\pi(x)$, which is well approximated by the "integral logarithm" [9] $\pi(x)\approx\int_2^x\frac{dx'}{\ln x'}$. The average particle density of prime number and Ulam spiral arrays can be easily calculated by considering the normalized (per unit area) number of primes up to the square of the largest integer in the array n^2:

$$\rho\approx\frac{1}{L^2}\int_2^{n^2}\frac{dx'}{\ln x'} \tag{3}$$

where L is the linear dimension of the array. Therefore, even if the minimum interparticle distance is the same in each array, prime number and Ulam arrays have a much lower density than the corresponding periodic arrays due to the logarithmic distribution of primes. Moreover, their density decreases as the linear dimension of the structures increases. The theoretically estimated densities of the different arrays, calculated as described above, are tabulated together with the exact densities of the arrays in Table 1. In the same table, we also list the linear dimensions of the arrays (L), the filling fractions (FF) of the arrays, the average nearest neighbor distance between nanoparticles ($<d_{min}>$), and the minimum interparticle separations (d_{min}). We notice that all the arrays have been generated with a comparable number of nanoparticles, as shown in Table 1.

3. Broadband plasmonic field enhancement in prime number arrays

In this section, we will study the near-field enhancement behavior of prime number arrays and we will discuss it in relation to the nature of their Fourier spectra and densities (the particles filling fractions). In Fig. 3(a), we show the calculated spectra of the electric field enhancement for all the different structures, immersed in air. The case of a single Ag nanosphere of 50nm radius is also shown for comparison. In Fig. 3 (a), for each frequency in the visible spectrum we plot the maximum value of the electric field magnitude probed in the arrays plane, normalized to the value of an incident plane wave. To better describe the influence of both the polarization states of the incident field, we have excited the arrays using a circularly-polarized plane wave at normal incidence. The results shown in Fig. 3(a) clearly

#116360 - $15.00 USD Received 27 Aug 2009; revised 9 Nov 2009; accepted 9 Nov 2009; published 18 Dec 2009

demonstrate the larger field enhancement achieved in aperiodic arrays, over a broader wavelength range compared to both the single Ag particle and the periodic lattice of identical (minimum) interparticle separation. It is important to notice that these results are obtained despite the lower filling fractions of prime number arrays.

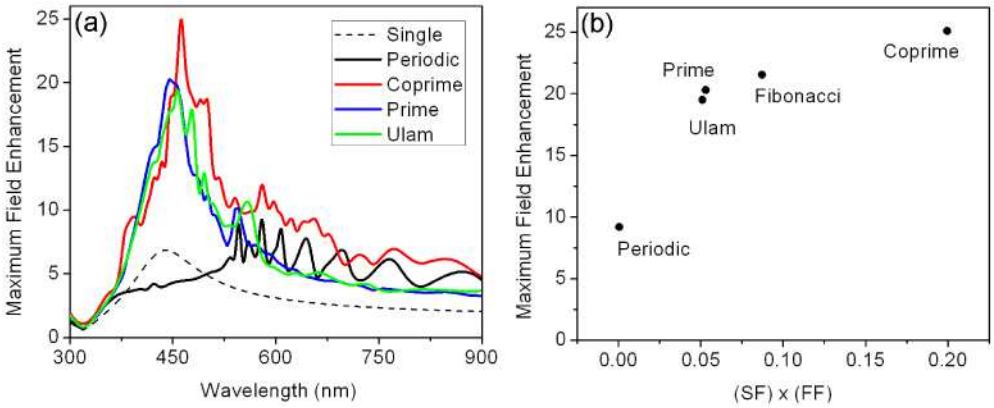

Fig. 3. (a) Maximum field enhancement versus the wavelength for an isolated particle, and for Periodic, Coprime, Prime, and Ulam arrays. The arrays are exited by a circularly polarized plane wave at normal incidence. (b) Values of maximum filed enhancement versus the spectral flatness (SF) – filling fraction (FF) product for the different arrays indicated in the figure.

The results in Fig. 3(a) can be qualitatively understood in light of the uncertainly principle for optical waves [25] complemented with the observation that plasmonic nanoparticles strongly couple at very short distances (quasi-static regime). The uncertainty principle states that the ultimate limit to the localization of any wave in a given direction Δx is uniquely dictated by the spread (uncertainty) in the corresponding wavevector components Δk_x, according to the well-known relation: $\Delta x \geq \alpha/\Delta k_x$ where α is a constant. It follows that this principle, if the Fourier spectrum of a plasmonic array is almost flat (large value of spectral flatness), a large number of spatial frequencies (wavenumbers) are available to match in-plane scattering processes resulting in efficient multiple scattering in the array plane.

However, not all the spatial frequencies in the Fourier spectral bandwidth will give rise to plasmon localization and enhancement effects. In fact, plasmon waves couple very strongly only in the near-field regime at very short distances, and a close nanoparticles packing is also needed in order to achieve high values of field enhancement. As a result, the aperiodic structures which possess both large spectral flatness SF and nanoparticle filling fraction (FF) will result in strong plasmonic scattering and near-field plasmonic localization. In order to validate this physically intuitive guiding principle, we have defined a figure of merit consisting of the SF-FF product, and we have plotted it for the different arrays in Fig. 3(b). Calculation results on a Fibonacci quasi-periodic array with comparable particle number (1428) and the same minimum interparticle separation (25nm) are also included for comparison. Our results demonstrate that the coprime array, which shows the best performance, also maximizes the SF-FF product due to its unique combination of large structural disorder and large particle filling fraction. On the other hand, despite the prime number and Ulam arrays feature an even larger spectral flatness, their particle filling fraction is significantly smaller than the coprime case, limiting the plasmonic performances.

#116360 - $15.00 USD Received 27 Aug 2009; revised 9 Nov 2009; accepted 9 Nov 2009; published 18 Dec 2009

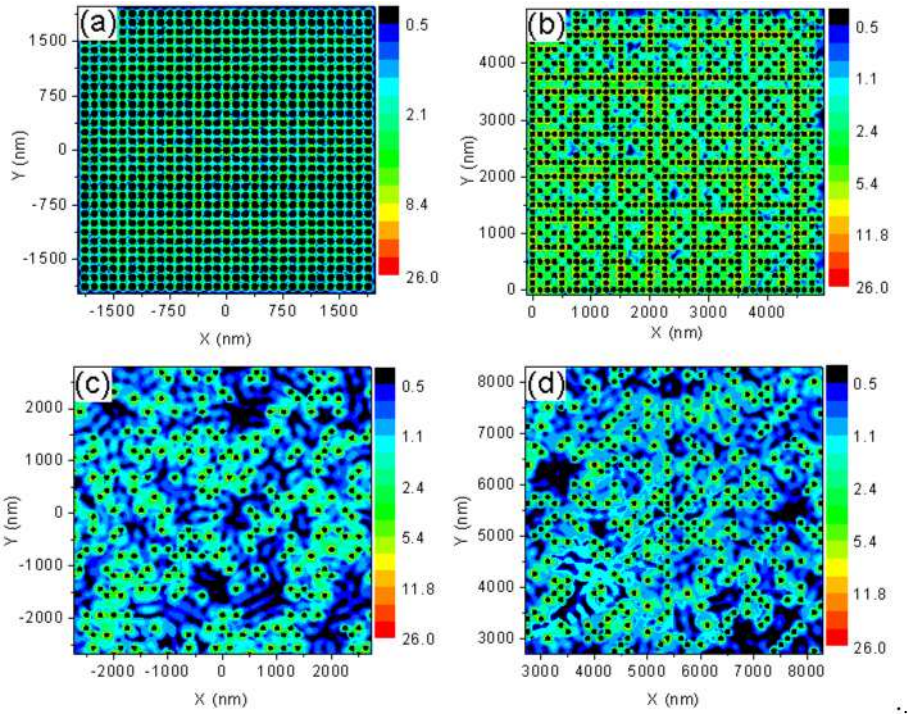

Fig. 4. Field enhancement spatial distribution (logarithmic scale) on the array's plane at the frequencies of the maximum field enhancement: (a) periodic at 580nm (b) Coprime at 462nm (c) Prime at 439 nm (d) Ulam at 450 nm. The arrays are exited by a circularly polarized plane wave at normal incidence.

The field enhancement oscillations observed for the periodic array (Fig. 3(a), black line) are related to its finite size, which makes possible the excitation of structural resonances with field enhancement [26]. These finite size resonances are not visible for aperiodic arrays due to their larger structural disorder, which makes them less sensitive to the coherent interactions (multiple interference effects) involving the boundaries of finite-size structures.

The unique interplay between near-field plasmonic coupling and long-range multiple scattering for prime number structures is clearly displayed in Fig. 4 where we show the electric field spatial distribution at the wavelengths of the enhancement peak (Fig. 3(a)). The field distributions of the prime number and Ulam arrays show the presence of well-isolated nanoparticle clusters (along the diagonals) strongly coupled in the quasi-static (near-field) regime. In addition, the highly inhomogeneous field distributions in Fig. 4(b)-4(d)) demonstrate the importance of long-range diffractive coupling (multiple scattering) effects in the plane of the array, which couple all the particle clusters in the aperiodic arrays. On the other hand, in the case of the periodic array shown in Fig. 4 (a), the nanoparticles are prevalently coupled in the near-field regime, with strongly reduced phase modulation across the array plane. In this case, extended plasmonic structural resonances, analogous to the Fabry-Perot-type modes in finite-size structures are formed [26]. On the opposite, due to the increased structural disorder (spectral flatness), the nanoparticles in the aperiodic arrays are strongly coupled in both the plasmonic near field regime and the photonic diffractive one (long-range coupling), resulting in strong in-plane multiple light scattering. The coexistence of different electromagnetic coupling regimes at multiple length scales is at the origin of the superior field enhancement and localization observed in several aperiodic plasmonic structures [1,2,15].

#116360 - $15.00 USD Received 27 Aug 2009; revised 9 Nov 2009; accepted 9 Nov 2009; published 18 Dec 2009

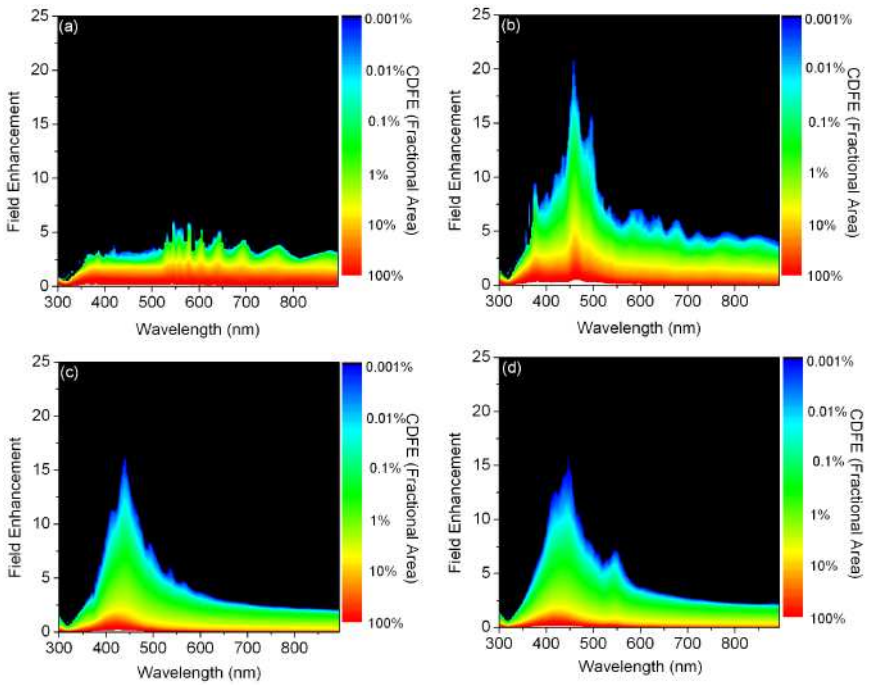

Fig. 5. The color-maps show the cumulative distributions of field enhancement (CDFE) (logarithmic scale) versus wavelength (x-axis) and field-enhancement (y-axis) for (a) Periodic (b) Coprime (c) Prime and (d) Ulam arrays. The arrays are excited by a circularly polarized plane wave at normal incidence.

Another very important aspect of the considered prime number plasmonic arrays relates to the fraction of the total array area covered by strong plasmonic fields. In plasmonic sensing technology, the understanding of the area density of enhanced fields on a planar chip is of fundamental importance. In order to quantitatively understand this aspect, we studied the fraction of the total area of the arrays covered by plasmonic enhanced fields with values greater then a fixed threshold. This important feature is mathematically defined by the cumulative distribution of field enhancement (CDFE) which we have recently introduced for aperiodic arrays [15]. In Fig. 5 we show the CDFE plots for the different arrays.

For a given wavelength (x-axis) the CDFE function represents (in colors) the fraction of total area of the array covered by field values greater then a fixed value (shown on the y-axis). This function concisely displays all the relevant plasmonic behavior of the different arrays. In particular, we can see in Fig. 5(a) that the maximum value of the field enhancement of the periodic array is roughly 10 (Fig. 3(a)), but values of field enhancement larger than 6 only cover a total area of the periodic array less than $\sim 0.001\%$. On the other hand, in the case of aperiodic structures (Fig. 5(b)-5(d)), values of field enhancement larger than 5 cover $\sim 1\%$ of the coprime, $\sim 0.1\%$ of the prime and Ulam arrays. Moreover the highest value of field enhancement (up than 20 for coprime, 15 for prime and Ulam) are strongly localized in a region $\sim 0.01\%$ of their total array areas. Therefore, based on our analysis we conclude that aperiodic arrays with large spectral flatness and particle filling fraction values give rise to strongly enhanced field states over larger array areas compared to periodic plasmonic structures.

#116360 - $15.00 USD Received 27 Aug 2009; revised 9 Nov 2009; accepted 9 Nov 2009; published 18 Dec 2009

4. Fourier space engineering and far-field scattering from aperiodic arrays

So far, we have demonstrated that the large number of spatial k vectors associated to the spectral flatness of aperiodic structures plays a crucial role in improving the plasmonic near-field performances of nanoparticle arrays.

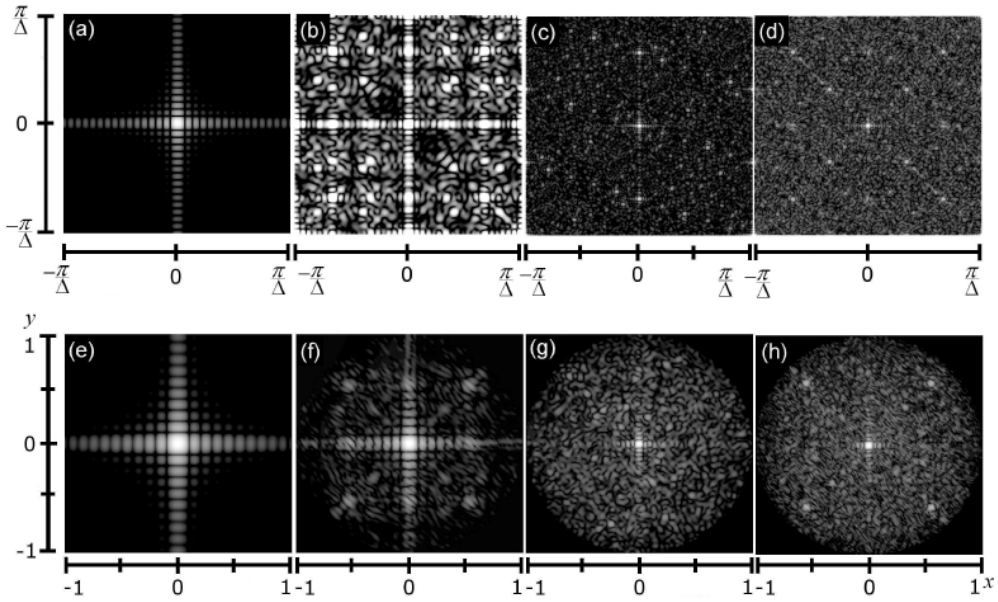

Fig. 6. Reciprocal lattice (logarithmic scale) (a-d) compared to the scattering maps (logarithmic scale) for the forward scattering hemisphere (e-h) for: (a) and (e) Periodic, (b) and (f) Coprime, (c) and (g) Prime, (d) and (h) Ulam arrays. The arrays are excited by a circularly polarized plane wave at normal incidence and at the wavelength of the maximum of scattering efficiency, i.e. (a) 389.5nm, (b) 462nm, (c) 439nm, (d) 450.5nm. The scattering angles can be calculated from the *horizontal* and *vertical* axes values as $\cos^2\theta = \max\{0,1-x^2-y^2\}$, $\varphi = \tan^{-1}(y/x)$.

It is also very interesting to study the behavior of plasmonic aperiodic structures in the far-field scattering zone, particularly in relation to the possibility of designing the radiation patterns of complex nano-antenna arrays for nanoplasmonics applications [27, 28]. In Fig. 6(e)-6(h) we show the calculated scattering maps [2] for the different arrays excited by a circularly polarized plane wave normally incident at the frequency of the maximum scattering efficiency. The scattering map representation, well known in the context of multiple scattering theories [29], represents the magnitude of the scattered field on the far-field hemisphere (in the forward direction) projected into a scattering plane parallel to the array plane. All the information on the angular forward scattering of the arrays is therefore contained in the scattering maps, as discussed in Ref. 2. In Fig. 6(a)-6(d) we display the magnitude of the Fourier spectra of the arrays. The similarity between the far-field scattering maps and the corresponding Fourier spectra of the arrays is evident in Fig. 6.

#116360 - $15.00 USD Received 27 Aug 2009; revised 9 Nov 2009; accepted 9 Nov 2009; published 18 Dec 2009

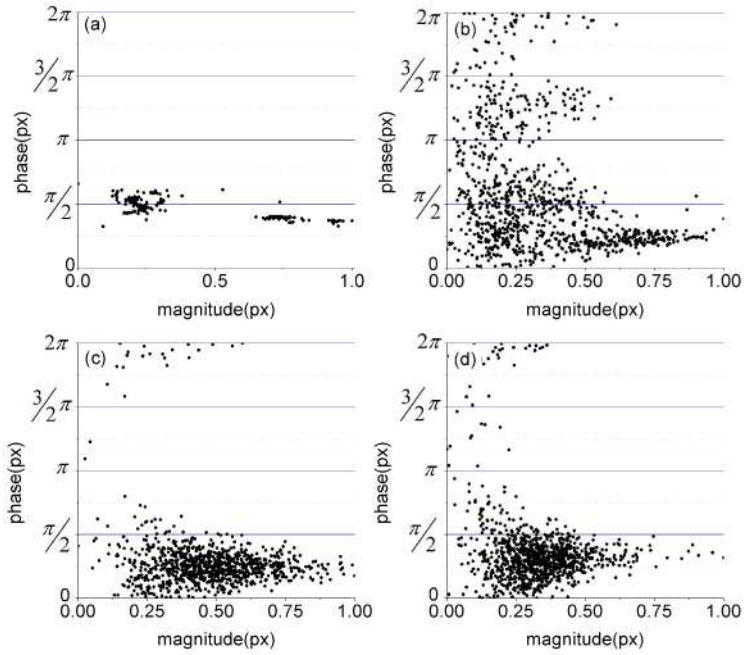

Fig. 7. Each scattered point represents the couple (magnitude, phase) of the projections of the dipolar moments along the polarization direction (x-axis) for Periodic (a), Coprime (b), Prime Numbers(c), and Ulam (d) arrays. These structures are excited by a x-polarized plane wave, at normal incidence, propagating at the wavelength of the maximum scattering efficiency, i.e. (a) 580nm, (b) 462nm, (c) 439nm, (d) 450nm. The magnitude is normalized to the maximum in each case (i.e. (a) $2.5\cdot10^{-32}$, (b) $8.6\cdot10^{-32}$, (c) $1.0\cdot10^{-31}$, and (d) $5.6\cdot10^{-32}$).

In addition, our computational analysis has evidenced that, if we increase the interparticle distance, the scattering maps resemble even more closely the Fourier transforms of the lattices. Therefore, by increasing the interparticle distance we observe a transition form a "plasmonic regime", where particles are strongly coupled in the near-field, to a "photonic regime" where the interparticle interactions are weaker and the far field maps approach the Fourier transforms of the lattices. It is interesting to notice that in this regime, despite the strong dispersion and losses introduced by the Ag nanoparticles, simple design criteria based on standard Fourier optics can be applied even to plasmonic nano-antenna arrays. This simple picture breaks down in the presence of strong interparticle plasmonic coupling, where more rigorous vector calculations are needed. In the case of the nano-plasmonic arrays considered in this paper, we indeed observe clear deviations from the simple Fourier optics picture especially for the coprime lattice (Fig. 6 (b)-6(f)). In the following, we will discuss the validity of Fourier-space engineering design criteria for nanoplasmonic antenna arrays in more detail.

In order to understand in all generality the relation between the scattered far-fields and the Fourier spectra of aperiodic arrays we remember that, for an array of N point dipoles p_i, the scattered far-field is given by [30]:

$$\vec{E}(\vec{r}) \approx \frac{1}{4\pi\varepsilon_0} k^2 \frac{\exp(jkr)}{r} \vec{A} \sum_{i=1}^{N} \exp\left(jk\hat{r}\cdot\hat{r}_i\right)\vec{p}_i \qquad (4)$$

where k is the wavenumber, ε_0 is permittivity of the space, and $\vec{A} = -\hat{r}\times\hat{r}\times(\cdot)$ is a projection operator.

#116360 - $15.00 USD Received 27 Aug 2009; revised 9 Nov 2009; accepted 9 Nov 2009; published 18 Dec 2009

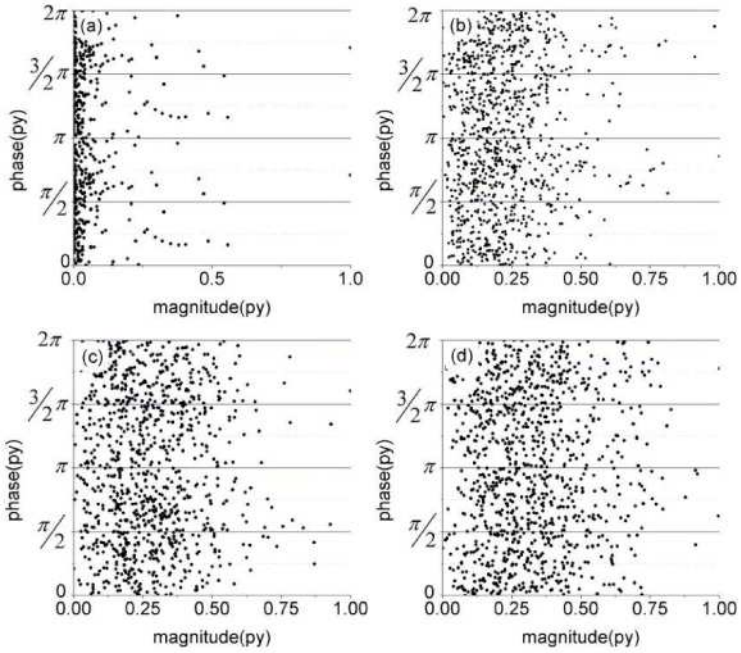

Fig. 8. Each scattered point represents the couple (magnitude, phase) of the projections of the dipolar moments along the vertical array's axis (y-axis) for (a) Periodic, (b) Coprime, (c) Prime Numbers, and (d) Ulam arrays. These structures are excited by a horizontal-polarized plane wave, at normal incidence, propagating at the wavelength of the maximum scattering efficiency, i.e. (a) 580nm, (b) 462nm, (c) 439nm, (d) 450nm. The magnitude is normalized to the maximum in each case (i.e. (a) $6.79 \cdot 10^{-33}$, (b) $4.6 \cdot 10^{-32}$, (c) $4.8 \cdot 10^{-32}$, and (d) $1.25 \cdot 10^{-32}$) .

Equation (4) shows that the scattered far field is directly proportional to the array factor of the nano-antenna array modulated by the phases of the dipoles.

If all the dipoles have the same magnitude and the same phase, Eq. (4) reduces to:

$$\vec{F}(\vec{r}) \approx \frac{1}{4\pi\varepsilon} k^2 \vec{A} \sum_{i=1}^{N} \exp\left(jk\hat{r} \cdot \vec{r}_i \right) \vec{p} \tag{5}$$

By defining the positions of all the dipoles with the functions:

$$\varphi(\vec{x}) : R^3 \longrightarrow \begin{cases} ¥ \;\; if \;\; \vec{x} \hat{I} \left\{ \vec{r}_i \;\; i = 1, 2, ... N \right\} \\ 0 \qquad\qquad otherwise \end{cases} = \sum_{i=1}^{N} \delta\left(\vec{x} - \vec{r}_i \right) \tag{6}$$

We can easily recognize that Eq. (5) is equivalent to:

$$\vec{F}(\vec{r}) \approx \frac{1}{4\pi\varepsilon} k^2 \vec{A} \vec{p} \iiint_{R^3} \varphi(\vec{x}) \exp\left(jk\hat{r} \cdot \vec{x} \right) dx = \frac{1}{4\pi\varepsilon} k^2 \Phi\left(k\hat{r} \right) \vec{A} \vec{p} \tag{7}$$

where Φ is the Fourier transform of φ. Eventually, by taking the Euclidean norm of both sizes of (7) we obtain:

$$\left\| \vec{F}\left(k\hat{r} \right) \right\|_2 = const \cdot k^2 \left| \Phi\left(k\hat{r} \right) \right| \tag{8}$$

which demonstrates that, if the dipoles have equal amplitudes and phases, the magnitude of the far-field scattered by the nanoplasmonic arrays is proportional, at any given frequency, to the Fourier transform of the arrays. This result justifies simple Fourier-space engineering design criteria in the context of plasmonic nano-antennas. In Figs. 7 and 8 we plot the

#116360 - $15.00 USD Received 27 Aug 2009; revised 9 Nov 2009; accepted 9 Nov 2009; published 18 Dec 2009

magnitudes and phases of the dipoles in the plane of the arrays calculated along the incident polarization direction (x) and along the orthogonal direction (y). These results have been obtained using a linearly polarized plane wave (at normal incidence) in order to better understand the role of dipole coupling along the two orthogonal directions x and y. Figure 7 demonstrates that, in the case of periodic, prime and Ulam arrays, the dipoles with the largest magnitudes cluster around a fixed phase value (Fig. 7(a), 7(c) and 7(d)), while the dipolar phases of the coprime lattice are somewhat scattered in the phase plane.

This confirms the important role played by the in-plane multiple scattering in coprime lattice, and explains the deviation from the simple Fourier optics picture. On the other hand, a direct evidence of enhanced in-plane multiple scattering for all the aperiodic arrays is given by the almost randomized dipolar phases observed in the direction perpendicular to the incident polarization (Fig. 8(b)-8(d)).

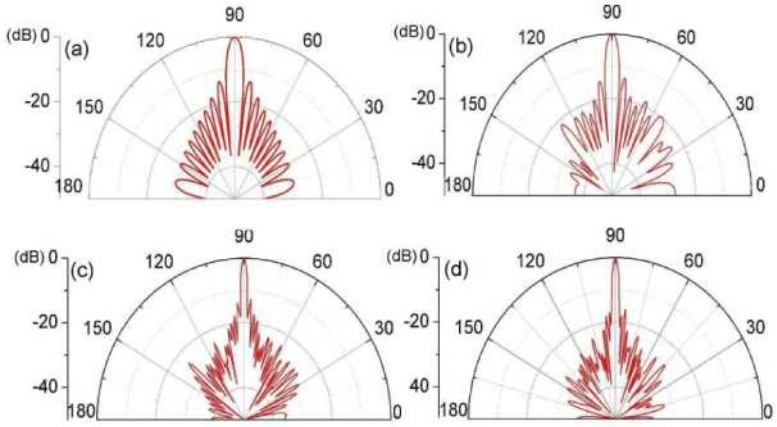

Fig. 9. Magnitude, in the Fraunhofer zone, of the scattered E-field in a plane orthogonal to the array and including the lattice's vertical axis, for different geometries, excited by a plane wave, propagating at the wavelength of the scattering efficiency's maximum: (a) Periodic at 580nm (b) Coprime at 462nm (c) Prime at 439 nm (d) Ulam at 450 nm. The incoming plane wave is at normal incidence and is circularly polarized. The plots are in dB scale.

The angular distribution of the scattered radiation in a specific plane is described by radiation diagrams (angular diagram of the scattered fields), which can be directly obtained from the scattering maps [29]. In Fig. 9 we plot the angular diagram of the scattered field in a plane orthogonal to the array, obtained directly from the scattering maps in Fig. 6 by a line cut along a vertical axis passing through the center. In Fig. 11 we display the angular scattering diagram in the array plane. These diagrams are the analogue, limited to the scattered field, of the radiation polar diagrams obtained for the total field generated by antenna arrays in the RF regime. In the context of light scattering from plasmonic nano-antenna arrays, these plots give quantitative information on the angular scattering profile of incident radiation in a given plane.

#116360 - $15.00 USD Received 27 Aug 2009; revised 9 Nov 2009; accepted 9 Nov 2009; published 18 Dec 2009

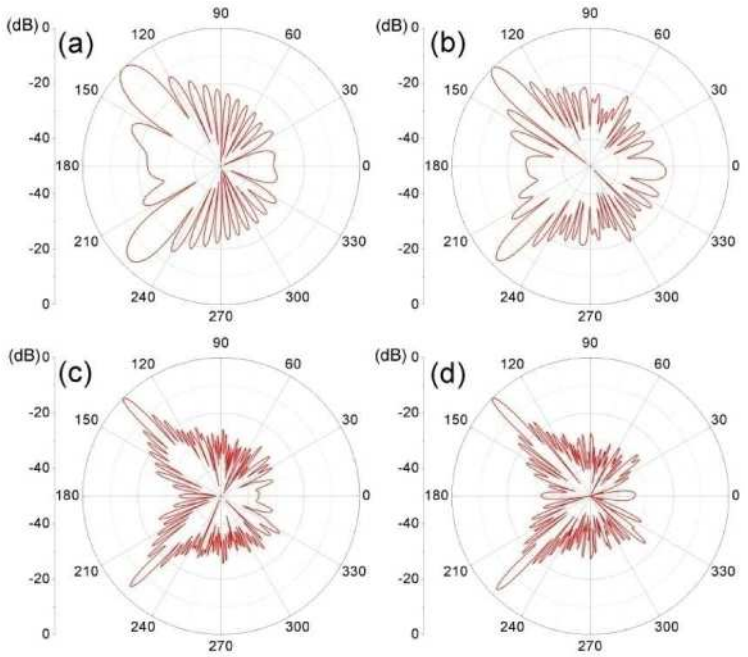

Fig. 10. Magnitude, in the Fraunhofer zone, of the scattered E-field in a plane orthogonal to the array and including the lattice's vertical axis, for different geometries, excited by a plane wave, propagating at the wavelength of the scattering efficiency's maximum: (a) Periodic at 580nm (b) Coprime at 462nm (c) Prime at 439 nm (d) Ulam at 450 nm. The incoming plane wave is at 45° incidence and is circularly polarized. The plots are in dB scale.

We notice in Fig. 9(a) that the out-of-plane scattering of periodic plasmonic arrays feature well-defined grating lobes due to the periodicity of the structure. These lobes are strongly suppressed in aperiodic arrays because of the increased structural "disorder" (spectral flatness) which prevents the formation of periodic grating modes, as shown in Fig. 9(b)-9(d). Interestingly, the out-of-plane scattering diagrams in Fig. 9 demonstrate that the angular width of the forward scattering lobe decreases by reducing the symmetry of the arrays from periodic to aperiodic. This behavior can be described quantitatively by the introduction of the parameter δ which measures the directionality of the scattered field intensity along the direction of maximum scattered intensity:

$$\delta = 10\log_{10}\frac{\max_{\vartheta,\varphi}\left|E_S^2(\vartheta,\varphi)\right|}{\frac{1}{4\pi}\int_0^{2\pi}d\varphi\int_0^{\pi}d\vartheta\left|E_S^2(\vartheta,\varphi)\right|\sin(\vartheta)} \tag{11}$$

where ϑ, φ are the polar and azimuthal angle; $E_S(\vartheta,\varphi)$ is the scattered electric field along the direction specified by the angles ϑ,φ. Additionally we calculated the angular width at half maximum Δθ of the scattered far-field intensity around the direction of maximum scattering. These scattering parameters are listed for all the arrays in Table 2.

These values demonstrate that the investigated aperiodic arrays feature an enhanced directional forward scattering compared to the reference periodic array. It is important to note that both the amplitude and the angular width of the forward scattering lobes of prime number arrays decrease by increasing their structural complexity. However, the width of the scattering lobes of prime number structures is also directly affected by their larger geometrical size, which modifies the associated reciprocal lattices by a convolution with a narrower sinc function.

#116360 - $15.00 USD Received 27 Aug 2009; revised 9 Nov 2009; accepted 9 Nov 2009; published 18 Dec 2009

Table 2. – The directional parameter δ and the angular width at half maximum Δθ are reported for Periodic, Coprime, Prime and Ulam spiral when the array is excited by a circular polarized plane wave at normal incidence, propagating at the wavelength of the maximum scattering efficiency.

	Periodic	Coprime	Prime	Ulam
δ (dB)	33	35	79	75
Δθ (degree)	2.9	2.9	1.4	1.4

It is interesting to notice that, the lobes corresponding to transmitted and reflected radiation dominate the scattering diagrams when the incident wave is illuminating the arrays at oblique incidence (45°), as shown in Fig. 10.

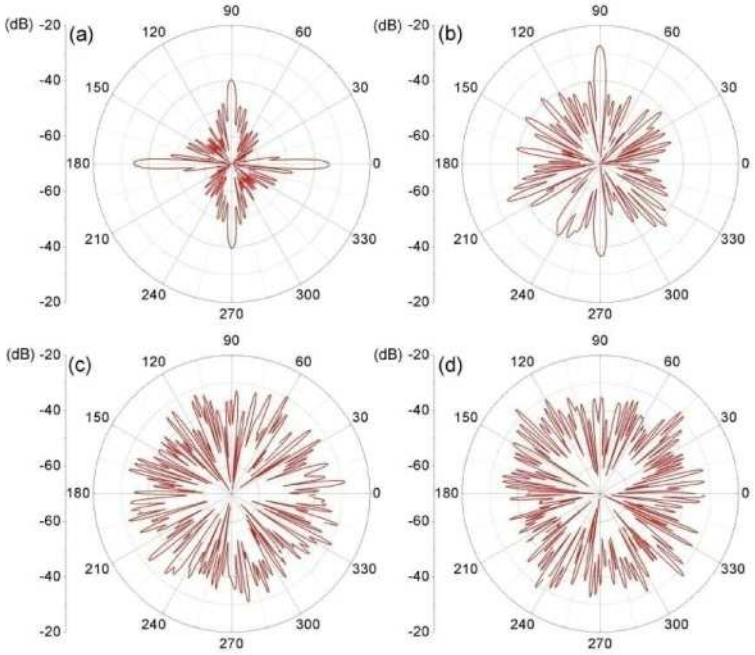

Fig. 11. Magnitude, in the Fraunhofer zone, of the scattered E-field in the array's plane, for different lattices excited by a plane wave at the frequencies of the scattering efficiency's maxima: (a) Periodic at 389.5nm, (b) Coprime at 462nm, (c) Prime at 439nm (d), and Ulam at 450.5nm. The incoming plane wave has a wave vector orthogonal to the array's plane and is circularly polarized. The plots are in dB scale.

Our results demonstrate that also under the conditions of oblique incidence the grating lobes are strongly suppressed due to the "symmetry breaking" characteristic of aperiodic structures.

In Fig. 11 we show the angular distribution of the scattered radiation in the plane of the plasmonic arrays. In Fig. 11(a) clearly defined in-plane scattering directions can be identified for the periodic array in correspondence to the symmetry directions of the lattice. On the opposite, we notice in Fig. 11(b)-11(d) that the angular scattering of aperiodic arrays (in the plane of the arrays) becomes almost isotropic as the spectral flatness increases from coprime to prime number arrays, although the intensity in the plane of the array is appreciably lower than the intensity in the forward direction. As expected based on their Fourier spectra, the in-plane scattering diagrams of prime and Ulam spiral arrays (Fig. 11(c) and 11(d)) approximate the behavior of isotropic scatterers with no identifiable symmetries (compare with Fig. 6(g) and h).

#116360 - $15.00 USD Received 27 Aug 2009; revised 9 Nov 2009; accepted 9 Nov 2009; published 18 Dec 2009

The unique out-of-plane and in-pane scattering behavior of prime number plasmonic arrays with large spectral flatness could suggest novel engineering strategies for more efficient solar absorbers and compact detectors.

Conclusions

In this paper, we have investigated the near-field plasmonic behavior and the far-field scattering characteristics of aperiodic arrays of Ag nanoparticles based on the distribution of prime numbers in two spatial dimensions. In particular, we have demonstrated that the engineering of compact arrays with large spectral flatness is necessary to achieve a high density of electromagnetic hot spots distributed over a broader frequency range and a larger array area compared to strongly coupled periodic and quasi-periodic structures. Finally, we studied the far-field angular scattering properties of prime number structures and discuss simple design criteria of Fourier-space engineering for nanoplasmonic antenna arrays. The understanding of strongly coupled plasmonic arrays with large spectral flatness can result in the demonstration of novel nanoplasmonics elements such as nano-antenna arrays, active plasmonic structures and broadband-enhanced solar cells.

Acknowledgments

This work was partially supported by the DARPA-DSO Chemical Communication project (ARM168), the U.S. Army through the Natick Soldier Center (W911NF-07-D-001), the SMART Scholarship Program, the Air Force program “Deterministic Aperiodic Structures for on-chip nanophotonics and nanoplasmonics device applications” supervised by Dr. Gernot Pomrenke and by the EURATOM/ENEA/CREATE Association.

#116360 - $15.00 USD Received 27 Aug 2009; revised 9 Nov 2009; accepted 9 Nov 2009; published 18 Dec 2009